JOURNAL OF GEOPHYSICAL RESEARCH, VOL. 102, NO. A2, PAGES 2147-2155, FEBRUARY 1, 1997

Quantitative model of the Martian magnetopause shape and its variation with the solar wind ram pressure based on Phobos 2 observations

M. Verigin,[1] G. Kotova,[1] N. Shutte,[1] A. Remizov,[1] K. Szegö,[2] M. Tátrallyay,[2] I. Apáthy,[3] H. Rosenbauer,[4] S. Livi,[4] A. K. Richter,[4] K. Schwingenschuh,[5] T.-L. Zhang,[5] J. Slavin,[6] and J. Lemaire[7]

Abstract. A model of the Martian magnetopause is developed for the period of maximum solar activity which simultaneously describes (1) the observed relation between the solar wind ram pressure ρV^2 and the magnetopause position in the magnetotail, (2) the observed relation between ρV^2 and the flaring angle, and (3) a few magnetopause crossing observations above the day side of the planet. The shape of the magnetopause is determined from the equation of pressure balance across this boundary when both the magnetic pressure (with a planetary magnetic moment of $(0.8\text{-}1.0)\times10^{22}$ G cm^3) and the ionospheric pressure are taken into account in the planetary magnetosphere. The specific feature of the model is the "stagnation" of the subsolar magnetopause when the ram pressure increases to higher values ($\geq 6\times10^{-9}$ dyn cm^{-2}).

Introduction

Although 30 years have passed since the beginning of in situ studies of the near-Martian space (Mariner 4, 1965), Mars still remains the only visited planet of the solar system with uncertain information on its magnetic moment and on the role of the planetary ionosphere in the interaction with the solar wind. Since there are still no direct measurements of the magnetic field available near the surface of Mars, only indirect evidence can be used to come closer to the solution of the above problems. The studies of the variation of the position of planetary plasma boundaries, the magnetopause and the bow shock, being influenced by the solar wind ram pressure ρV^2 variations are among the useful diagnostic tools for analyzing these unsolved problems.

The attempts of *Slavin et al.* [1983] and *Schwingenschuh et al.* [1992] to study the dependence of the location of the Martian terminator bow shock on solar wind ram pressure did not lead to an indisputable conclusion on the origin of the planetary obstacle to the solar wind flow because of many uncontrolled factors which determine the position of this boundary. The number of external factors which control the magnetopause position is less than those controlling the bow shock. Also, the magnetopause is located closer to the planet. This means that the study of the magnetopause motions is a more sensitive tool for analyzing the nature of the obstacle to the solar wind.

[1]Space Research Institute, Russian Academy of Sciences, Moscow, Russia.
[2]KFKI Research Institute for Particle and Nuclear Physics, Budapest, Hungary.
[3]KFKI Atomic Energy Research Institute, Budapest, Hungary.
[4]Max-Planck-Institut für Aeronomie, Katlenburg-Lindau, Germany.
[5]Space Research Institute, Graz, Austria.
[6]NASA Goddard Space Flight Center, Greenbelt, Maryland.
[7]Belgisch Instituut voor Ruimte-Aeronomie, Brussels, Belgium.

Paper number 96JA01460.
0148-0227/97/96JA-01460$09.00

The compression of the Martian magnetotail with the increase of ρV^2 was qualitatively demonstrated by *Gringauz et al.* [1976a, b]. The first statistical study of this effect by *Verigin et al.* [1993] was based on the assumption of the relatively stable position of the magnetopause in the subsolar region which had no direct observational support. Later, *Rosenbauer et al.* [1994] studied the average flaring angle of the Martian magnetotail along the Phobos 2 orbit while *Zhang et al.* [1994, 1995] analyzed its dependence on solar wind ram pressure. Both papers provided additional information on the shape of the planetary magnetopause.

The aim of this paper is to develop a model of the Martian magnetopause which simultaneously describes (1) the observed relation between ρV^2 and the magnetopause position in the magnetotail, (2) the observed relation between ρV^2 and the flaring angle, and (3) a few magnetopause-crossing observations above the dayside of the planet.

Instrumentation and Observational Data

This model is based on the plasma proton component measurements performed by the TAUS spectrometer and magnetic field data measured by the MAGMA magnetometer onboard Phobos 2. In most of the Martian orbits during February - March 1989, the TAUS spectrometer measured proton spectra every 2 min in the energy per charge range of 150 V to 6 kV subdivided into 32 energy channels. The instrument had a field of view of $\sim 40^\circ \times 40^\circ$ centered on the nominal aberrated solar wind direction. A more detailed description of the TAUS instrument was presented by *Rosenbauer et al.* [1989a]. Most of the time, the MAGMA magnetometer measured the magnetic field vector every 45 s, with a resolution of 0.05 nT. Field values ranged between ±100 nT [*Aydogar et al.*, 1989].

During the active life of this orbiter, magnetopause crossings were observed by both TAUS and MAGMA instruments in three elliptical orbits with low pericenter ($h\approx850$ km above the planet's surface) and in several dozen circular orbits (planetocentric distance $r\approx9500$ km) quasi-synchronous with the orbit of the Phobos moon. Altogether 64 entries to the magnetotail or exits from

it (in the case of multiple crossings the innermost one was considered; see also the end of the next section and the discussion section) were recorded in the circular orbits for which both proton and magnetic measurements were available both in the solar wind and in the magnetotail lobes. The crossings of the magnetopause near Mars were indicated by the disappearance of solar wind protons as measured by TAUS [*Rosenbauer et al.*, 1989b] and by an increase in the magnitude of the magnetic field (in the magnetotail region) or by a drop in magnetic field turbulence (in the subsolar magnetosphere) [*Riedler et al.*, 1989].

It is obvious that for the magnetopause modeling, the absolute measurements of solar wind proton parameters and correct information on their accuracy play a crucial role. The efficiency of the proton channel (P) of TAUS systematically decreased during the mission owing to the incomplete opening of the exit slit by a charged piezoelectric actuator [*Verigin et al.*, 1993]. Postcalibration of channel efficiency was performed using proton ghosts in the heavy ion channel (H) where the slit was continuously open.

Figure 1 presents the inflight variation of the ratio of the number of protons N_p counted daily in the peak of P channel energy spectra to the number of protons N_h counted daily at the same energy in the H channel. The general trend of the count ratio can reasonably be approximated by the following exponential curve [*Kotova*, 1993]:

$$N_p/N_h = 18.08 + 81.84\exp(-0.01806t), \quad (1)$$

where t is the time measured in days from July 1, 1988. As one can see from Figure 1, the scatter of the individual points relative to the smooth curve (1) still leaves a rather large uncertainty in the postflight data correction procedure.

In order to adjust TAUS measurements to the long term multispacecraft data set systematically published by WDC-A in the Interplanetary Medium Data Books, the proton number densities determined by the IMP 8 MIT Faraday cup measurements [*King*, 1989] and those measured by TAUS were compared for the interval from September 21 to October 3, 1988 when the Sun, the Earth, and Phobos 2 were radially aligned. (See also work by

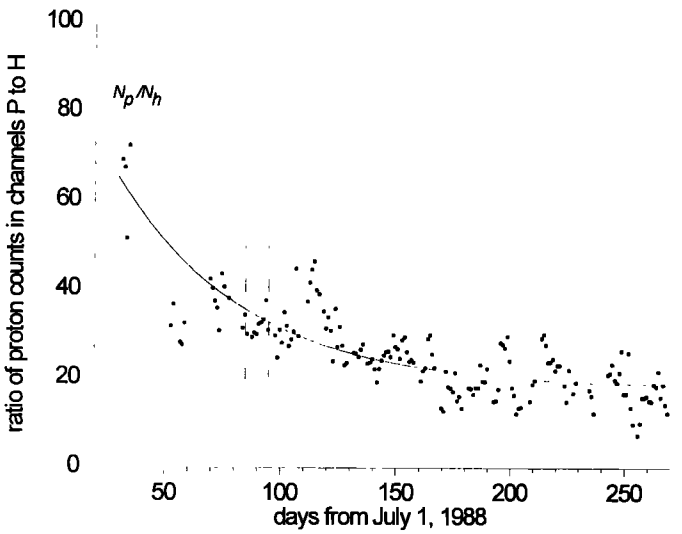

Figure 1. In-flight variation of the ratio of the number of protons counted daily at the peak of the proton channel energy spectra to the number of protons counted daily at the same energy in the heavy ion channel. Smooth curve approximation by expression (1). Vertical dashed lines mark the interval used for intercalibrations with IMP 8.

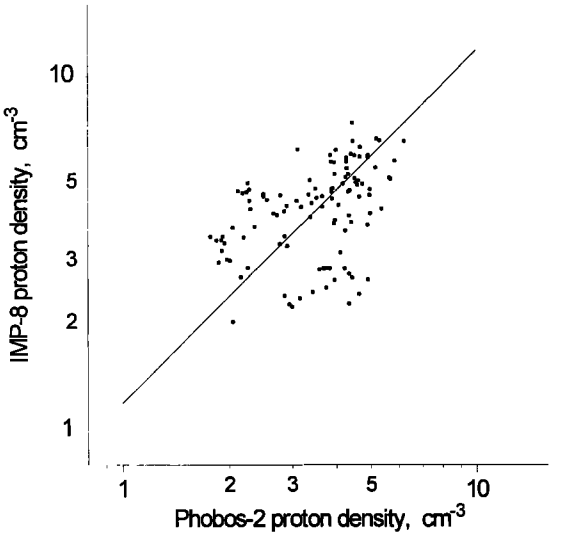

Figure 2. Intercomparison of Phobos 2/TAUS and IMP 8 solar wind proton densities.

Russell and Petrinec [1992]; and *Petrinec and Russell* [1993b] and ensuing commentary [*Paularena and Lazarus*, 1994; *Petrinec and Russell*, 1994] for discussion on certainty of IMP 8 data.) The delay time of the solar wind stream from IMP 8 to Phobos 2 was calculated by assuming that the velocity is independent of the heliocentric distance R. Only those 10-min averaged intervals were taken into account for which the solar wind velocity V measured by Phobos 2 was coincident with the velocity observed by IMP 8 within 10% accuracy. Then IMP 8 proton densities were adjusted to the position of Phobos 2 assuming the $\sim R^{-2}$ radial variation of this parameter.

Figure 2 shows the scatter plot, described above, of Phobos 2 proton density measurements relative to IMP 8 data. A least squares fit to the data in Figure 2 gives a multiplicative factor of 1.19 by which the Phobos 2/TAUS proton number density n_p (based on preflight calibrations) must be multiplied to match corresponding solar wind data from IMP 8. Then with the use of curve (1), the correction coefficient for TAUS data can be calculated for any period of time. Towards the end of the active life of Phobos 2, this coefficient turned to be about 2.2. Phobos 2/TAUS data corrected by this procedure were used earlier for the studies of the Martian magnetopause and bow shock variations and magnetotail properties [*Verigin et al.*, 1993; *Rosenbauer et al.*, 1994; *Zhang et al.*, 1994, 1995].

The values of V, n_p (adjusted), and proton temperature T_p measured by TAUS, and magnetic field B measured by MAGMA can be applied to estimate the solar wind ram pressure ρV^2 and thermal and magnetic field pressure p using the following relations:

$$\rho V^2 \approx n_p m_p V^2\left(1+\frac{n_\alpha}{n_p}\frac{m_\alpha}{m_p}\right),$$
$$p \approx n_p kT_p\left(1+\frac{n_\alpha}{n_p}\frac{T_\alpha}{T_p}+\left(1+\frac{2n_\alpha}{n_p}\right)\frac{T_e}{T_p}\right)+\frac{B^2}{8\pi}, \quad (2)$$

where m_p and m_α are the proton and α particle masses, respectively. The ratios of $n_\alpha/n_p \approx 0.047$, $T_\alpha/T_p \approx 4.9$, and $T_e/T_p \approx 1.9$ were adopted for the average solar wind properties according to *Feldman et al.* [1977].

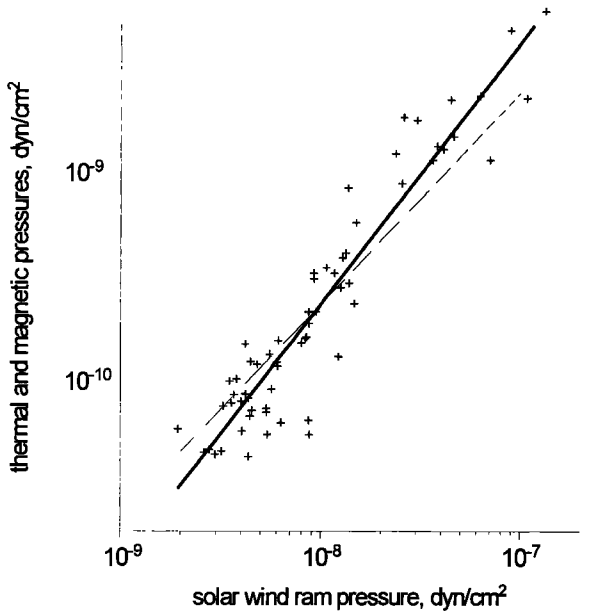

Figure 3. The scatter plot of p relative to ρV^2 upstream of the Martian bow shock in the period of Phobos 2 measurements.

Figure 3 presents the scatter plot of p relative to ρV^2 as measured by Phobos 2 in the solar wind upstream of each bow shock crossing averaged over time intervals of 20 to 30 min each beginning ~ 30 min after the outbound shock crossing and ending ~ 30 min before the inbound shock crossing [see *Verigin et al.*, 1993]. The solid line in this figure describes the best-fit power law dependence

$$p \approx 1.728\left(\rho V^2\right)^{1.232}, \tag{3}$$

which will be used in the following magnetopause modelling. The dashed line in Figure 3 corresponds to the magnetosonic number $M_{ms} \approx 4.6$ which characterizes the average conditions in the solar wind during the Phobos 2 measurements [cf. *Rosenbauer et al.*, 1994].

Magnetopause Model Construction

The equation of pressure balance across the magnetopause/ionopause is generally used for the theoretical determination of the obstacle shape both for magnetospheres produced by an intrinsic planetary dipole, and for magnetospheres induced by the solar wind-ionosphere interaction [*Spreiter et al.*, 1966, 1970]. One side of this equation usually includes the solar wind ram pressure ρV^2 and (sometimes) the solar wind thermal and magnetic field pressure p. The other side describes either the magnetospheric magnetic pressure (dipole magnetospheres) or the ionospheric plasma pressure (induced magnetospheres). Bearing in mind that in the case of the Martian magnetosphere both magnetic and ionospheric pressures might be important, we use the pressure balance equation with the sum of the above pressures on the right-hand side:

$$k\rho V^2 \sin^2\alpha + p = \frac{4f^2M^2}{8\pi r^6} + p_0 e^{-(r-r_0)/H}, \quad x > x^*$$
$$= \frac{B^{*2}}{8\pi}\left(\frac{y^*}{y}\right)^4, \quad x < x^* \tag{4}$$

where $x = x_{ase}$, $y = \sqrt{y_{ase}^2 + z_{ase}^2}$ are the magnetopause surface coordinates in the planetary-centered aberrated solar ecliptic coordinate system *ase* (x_{ase} is assumed to be antiparallel to the incoming solar wind direction), α is the flaring angle (between x_{ase} and the vector tangent to the magnetopause in the plane passing through x_{ase}), M is the magnetic moment of the planet, p_0 is the ionospheric pressure at distance r_0, H is the ionospheric pressure scale height, and $k \approx 0.88$ (for the ratio of specific heats $\gamma = 5/3$) and $f \approx 1.22$ ($f^2/k \approx 1.69$) are factors describing the transfer of the ram pressure to the subsolar magnetopause and the magnetic field amplification interior to the magnetopause by electric currents along this surface [*Spreiter et al.*, 1966; *Slavin and Holzer*, 1982], respectively.

After substituting $\sin^2\alpha$ via the dy/dx derivative into (4), the following differential equation was used for modeling the Martian magnetopause:

$$k\rho V^2 \frac{(y')^2}{1+(y')^2} + p(\rho V^2) = \frac{4f^2M^2}{8\pi r^6} + p_0 e^{-(r-r_0)/H}, \quad x > x^*$$
$$= \frac{B^{*2}}{8\pi}\left(\frac{y^*}{y}\right)^4, \quad x < x^* \tag{5}$$

where $p(\rho V^2)$ is taken from relation (3). In the planetary magnetotail ($x \le x^* \le 0$), (4) and (5) suggest the conservation of the magnetic field flux in the magnetotail lobes (parameters B^* and y^* obviously provide a smooth transition of the magnetopause surface at $x = x^*$). The value of $x^* = 0$ was adopted, which provides an approximate coincidence of the magnetopause shape determined from (5) for a purely magnetic obstacle with the "realistic magnetopause" by *Tsyganenko* [1995] based on the extensive statistical studies by *Sibeck et al.* [1991] and *Roelof and Sibeck* [1993]. The relation between the magnetotail width, the distance to the magnetopause in the terminator plane, and the subsolar magnetosphere dimension is 2.58:1.34:1 for the "realistic magnetopause" and 2.42:1.34:1 for the magnetopause obtained by integrating (5).

Once we select the values of the Martian magnetic moment M, the ionospheric pressure p_0, and the scale height H, equation (5) provides the expected position of the magnetopause surface and subsequently the distance from the observed magnetopause crossing to the expected surface for any observed value of the solar wind ram pressure ρV^2. The reverse problem is to find the parameters M, p_0, and H which minimize the deviation of the observed magnetopause crossings, from surfaces determined by our model and consistent with the measured parameters.

The amount of data available does not permit a three-dimensional (3-D) optimization study, especially in view of the small number of dayside magnetopause crossings. In fact, the three dayside crossings are responsible for the determination of p_0 and H, and any minor variation in the original dayside points leads to a serious change in the value of H. Therefore we fix the value of $H = 110$ km. This value is twice the scale height of the thermal oxygen in the maximal model of the Martian atmosphere of *Moroz et al.* [1991]. This model was selected since Phobos 2 measurements were performed near solar maximum. The influence of variations in H on the determination of other parameters is discussed later taking into account that the plasma scale height is twice the scale height of the ionizable constituent only under the condition of photochemical equilibrium [e.g., *Bauer et al.*, 1973], which may be violated in the upper ionosphere.

In a formal least squares optimization of fitting our model surfaces to observed magnetopause crossings, the 64 observations in

the magnetotail region would suppress the three dayside magnetopause crossings which, nevertheless, are very important for the subsolar boundary modeling. In order to "equalize" the significance of the magnetopause observations at the elliptic and circular orbits, we searched for the values of M and p_0 which provides the minimum of the sum of the mean squared deviations of the dayside observations and of the mean squared deviations of the tail observations (scaled to the subsolar point).

Figure 4 displays the results of the described optimization process for a value of $M = 0.815\times10^{22}$ G cm^3. In Figure 4a the solar zenith angles (arctan(y/x)) of the magnetopause crossings observed by Phobos 2 in circular orbits are shown as a function of ρV^2 compared with those expected from the model (smooth curve). In Figure 4b the smooth curve presents the expected relation between the height of the Martian magnetopause at the subsolar point and the solar wind ram pressure together with the three dayside magnetopause crossings traced to the $y = 0$ position along the proper model magnetopause surfaces. The model seems to reproduce the observed magnetopause crossings and their dependence on ρV^2 reasonably. (We do not present the optimum value of p_0 explicitly as it can easily be deduced from the exponential part of the smooth curve in Figure 4b which, according to (4) and (5), can be interpreted as the approximate height profile of the sum of the magnetic and ionospheric pressures in the subsolar region multiplied by the factor $1/k$.)

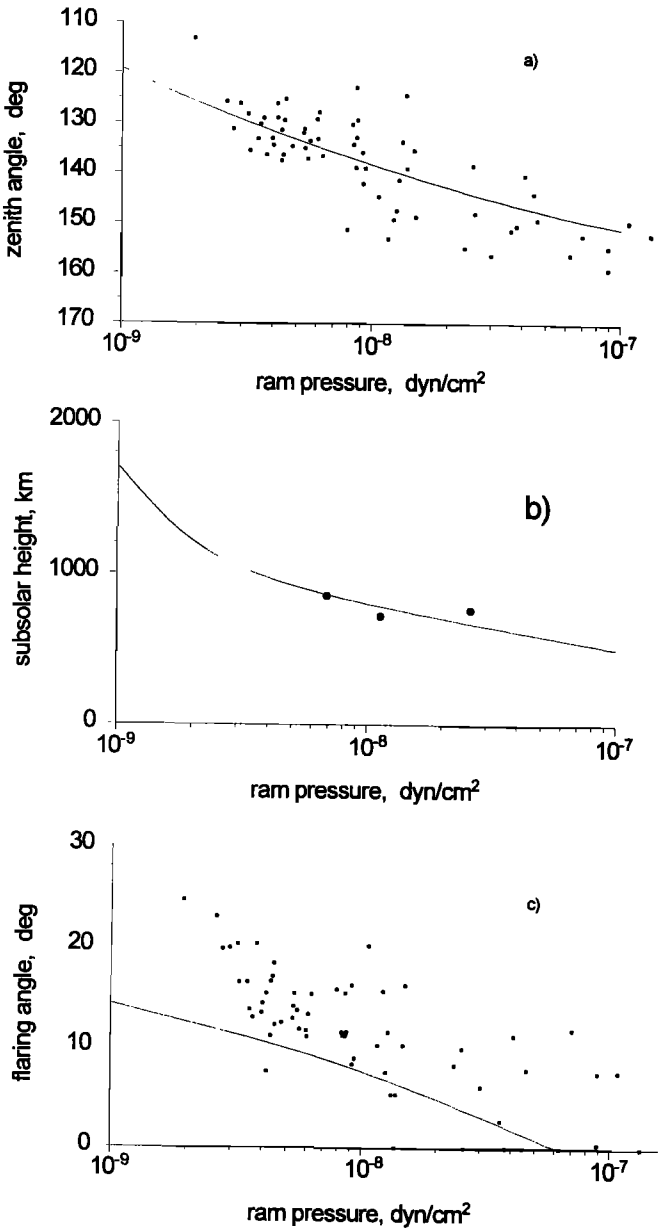

Figure 4. Comparison of the Martian magnetopause model for $M \approx 0.82\times10^{22}$ G cm^3 (smooth curves) with the observed magnetopause crossings at (a) circular orbits, (b) elliptic orbits, and (c) with magnetopause flaring angles deduced from Phobos 2 measurements.

A few additional runs of the model with $H \neq 110$ km were performed in order to study the influence of the uncertainty of this parameter on the evaluation of M. Varying H from 50 km to 200 km resulted in small changes in M from 0.84×10^{22} G cm^3 to 0.79×10^{22} G cm^3.

Up to this point, no information on the magnetotail flaring angles has been incorporated in the model. For a particular magnetopause crossing characterized by the solar wind upstream pressures ρV^2 and p, the Martian magnetotail flaring angle α can be determined as [cf. *Petrinec and Russell*, 1993a; *Zhang et al.*, 1994]

$$\sin^2\alpha = \frac{B_t^2/8\pi - p}{k\rho V^2}. \qquad (6)$$

Information on α is complementary to those shown in Figures 4a and 4b as it includes additional MAGMA measurements of the magnetic field in the Martian magnetotail lobes B_t. In order to determine B_t, we used those parts of the Phobos 2 orbits where the magnetic field reached a stable level in the magnetotail close to the innermost magnetopause crossing. The flaring angle thus determined is reasonable to be associated with the innermost crossing. Therefore only the innermost magnetopause crossings were used in Figure 4a also.

The scatter plot of flaring angles (as deduced from observations by relation (6)) versus ρV^2 is plotted in Figure 4c. The points are placed at 0° when $B_t^2/8\pi < p$. The values of the angles systematically exceed the model curve by 5°. No better agreement can be achieved by any variation of M or p_0. Some possible ways to avoid such a discrepancy will be presented in the discussion.

Discussion

As a consequence of the data presented in Figure 4 and as it was noted above, the developed model seems to reproduce the observed magnetopause crossings and their dependence on ρV^2 reasonably both in the subsolar region (Figure 4b) and in the tail region (Figure 4a). The magnetotail flaring angle dependence on ρV^2 (Figure 4c), however, is not reproduced satisfactorily by the model. The situation with the flaring angles may be improved either by modifying the theoretical background of the model or by varying the measured parameters of the magnetic field and/or plasma within the possible uncertainties of the observations.

In the first possible case the observational data would be reasonably reproduced by the model curves in all three panels of Figure 4 by selecting a value between $k = 1$ (diffuse reflection) and $k = 2$ (mirror reflection) [*Schield*, 1969] in (5) and (6). A reasonable result can be achieved for $k \approx 1.5$ and $M \approx 0.98\times10^{22}$ G cm^3. Although this is possible, there are more likely reasons for the differences between the model shapes and observations.

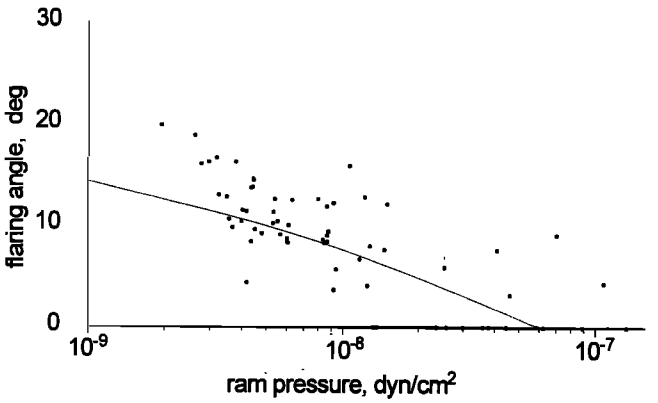

Figure 5. Comparison of the Martian magnetopause model for $M \approx 0.82 \times 10^{22}$ G cm^3 with magnetopause flaring angles deduced from Phobos 2 measurements when the tangential magnetic field component $B_{tt} \approx 0.85 B_t$ was used in relation (6).

A decrease of about 15% in the magnetic field values would also lead to a reasonable reproduction of all observational data by the model curves with about the same value of $M \approx 0.8 \times 10^{22}$ G cm^3. In this case the flaring angles of the particular crossings, as deduced from relation (6), are closer to the model curve in Figure 4c. Though the magnetic field measurements were beset with a zero-bias problem, it is difficult to believe that an offset correction of this size would be likely.

On the other hand, relation (6) should include the magnetic field component tangential to the magnetotail boundary B_{tt} rather than the absolute value of the magnetic field in the Martian magnetotail B_t. Substitution of $B_t \approx 0.85 B_t$ instead of B_t in relation (6) does not change the values of M and p_0 fitted earlier but results in a reasonable reproduction of the flaring angles by the model (Figure 5). This possibility conforms with the difference between flaring and draping angles in the Martian magnetotail found by *Zhang et al.* [1995].

A correction of the proton number density seems to be acceptable, too. If we draw the smooth curve approximating the N_p/N_h in-flight ratio about 30% below the curve shown in Figure 1 to the end of the Phobos 2 lifetime, the proton density values determined from the observation of the TAUS spectrometer will increase by about 40%. This possibility is not unrealistic taking into account the scatter of the N_p/N_h ratio in Figure 1 (see also Figure 2).

After correcting the proton number density by 40%, the quality of the correlation in Figure 3 does not change, but instead of relation (3) we obtain

$$p \approx 2.195 \left(\rho V^2\right)^{1.256} \qquad (7)$$

The optimization process, described in the previous section, with this new relation will lead to a new estimation of $M = 0.95 \times 10^{22}$ G cm^3. Figure 6 is similar to Figure 4, but it displays the modified model with the enhanced proton densities. This model seems to be another possibility (see model in Figures 4a, 4b and 5) to reproduce the observed magnetopause crossings and their ρV^2 dependences reasonably well both in the subsolar (Figure 6b) and tail region (Figure 6a) as well as the magnetotail flaring angle dependence on ρV^2 (Figure 6c).

The asterisk in Figure 6b marks the subsolar magnetopause altitude estimated by *Slavin et al.* [1993] based on magnetic field and plasma measurements on March 24, 1989. At this time, Phobos 2 observed the Martian bow shock close to the subsolar point, very far from the planet at ≈ 2.8 planetary radii as a result of the extremely low ram pressure $\rho V^2 \approx 10^{-9}$ dyn cm^{-2} and Alfvenic Mach number $M_a \approx 1.8$. The present model reproduces the estimated magnetopause position for very low solar wind ram pressure, thus implying that the effect of the planetary intrinsic magnetic field could be sufficient for the solar wind stagnation in this case.

Combination of both models presented in Figures 4a, 4b and 5 and Figure 6 (simultaneous moderate correction of B_t and n_p) also results in a reasonable reproduction of observations by the model. On the other hand, the incorporation of noninnermost

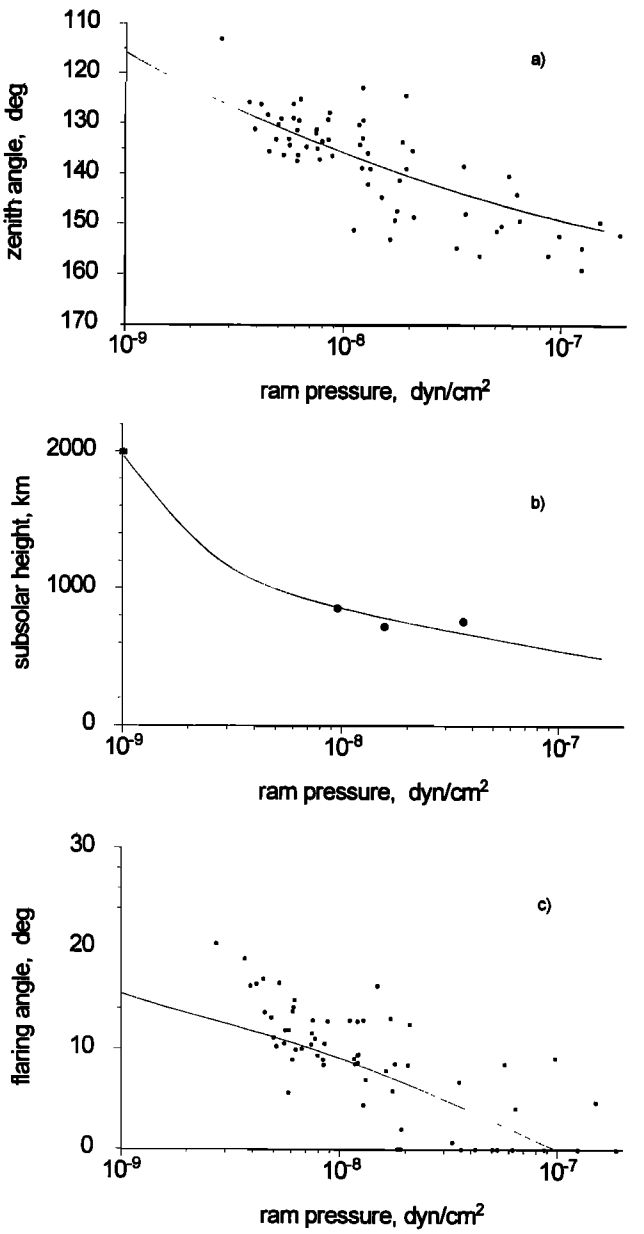

Figure 6. Comparison of the Martian magnetopause model for $M \approx 0.95 \times 10^{22}$ G cm^3 (smooth curves) with the observed magnetopause crossings at circular orbits (a), elliptic orbits (b), and with magnetopause flaring angles (c) deduced from Phobos 2 measurements after correcting the original solar wind proton density by a 40 % increase.

Table 1. Calculated Planetocentric Distances to the Model Magnetopause of Mars

Zenith Angle,	Solar Wind Ram Pressure, 10^{-9} dyn cm^{-2}					
deg.	1	2.3	6.3	16	40	100
	Planetocentric Distance, km ($M = 0.82\times10^{22}$ G cm^3)					
0	5102	4506	4271	4128	4011	3903
10	5118	4516	4276	4133	4016	3908
20	5167	4543	4290	4143	4025	3915
30	5249	4594	4316	4162	4042	3932
40	5370	4675	4356	4191	4066	3954
50	5536	4795	4416	4232	4101	3986
60	5753	4963	4507	4290	4148	4029
70	6031	5191	4645	4375	4213	4085
80	6387	5488	4851	4501	4304	4161
90	6844	5876	5146	4697	4437	4261
100	7468	6404	5570	5007	4662	4433
110	8375	7172	6200	5496	5044	4747
120	9722	8313	7141	6245	5647	5253
130	11803	10068	8592	7404	6584	6040
140	15225	12941	10953	9279	8083	7277
150	21451	18114	15148	12546	10619	9363
	Planetocentric distance, km ($M = 0.95\times10^{22}$ G cm^3)					
0	5371	4655	4336	4177	4055	3945
10	5388	4667	4342	4182	4060	3949
20	5439	4705	4359	4192	4068	3957
30	5528	4771	4389	4212	4085	3973
40	5656	4871	4437	4244	4112	3997
50	5831	5014	4512	4289	4148	4030
60	6060	5204	4624	4354	4198	4074
70	6354	5453	4792	4452	4268	4133
80	6731	5774	5032	4601	4369	4213
90	7217	6187	5364	4828	4521	4324
100	7879	6751	5829	5178	4775	4514
110	8844	7570	6511	5717	5194	4853
120	10280	8788	7530	6537	5849	5394
130	12502	10671	9102	7806	6870	6239
140	16179	13768	11675	9875	8517	7583
150	22935	19409	16307	13536	11360	9829

magnetopause crossings into the optimization procedure does not lead to an essential correction of the original model (Figure 4) because multiple magnetopause crossings were observed only for ~ 17% of 64 entries to the magnetotail or exits from it. In this case the value of the magnetic moment rises to $M \approx 0.9\times10^{22}$ G cm^3 while the model curves for ρV^2 dependences of zenith angle, subsolar height, and flaring angle differ from similar curves in Figures 4a-4c by < 3°, < 200 km, and < 1°, respectively.

The variation of the magnetopause shape as influenced by the variation of ρV^2 is very similar for both models presented in Figures 4(5) and 6. Table 1 presents the planetocentric distances to the magnetopause calculated from (5) as a function of ρV^2 and zenith angle for these models. Figure 7 shows a family of Martian magnetopause surfaces corresponding to the lower part of the Table 1. The short lines in Figure 7 are centered on the individual magnetopause crossings and inclined to the X axis at their individual α angles (6), thus demonstrating that the model fits are consistent with the deduced flaring angles.

As depicted in Figure 7, a specific feature of the model is the "stagnation" of the subsolar magnetopause with the increase of ram pressure for $\rho V^2 \geq 6\times10^{-9}$ dyn cm^{-2} while the magnetotail still remains compressible up to very large pressures. To some extent this behavior of the model magnetopause justifies the assumption of the stable position of the magnetopause in the subsolar region, used by *Verigin et al.* [1993] for the magnetotail compressibility study.

In the case of very low ρV^2, the magnetospheric magnetic field pressure $B^2/8\pi$ (first term in the right-hand side of (5)) dominates the ionospheric pressure p_{ion} (second term in the right-hand side of (5)) everywhere at the magnetopause in the model developed. Ionospheric pressure increasingly dominates magnetic pressure with increasing ρV^2 in the vicinity of the subsolar point. At larger zenith angles, however, the magnetic pressure still prevails owing to the slow ~ r^{-6} decrease of its value compared to the exponential decrease ~exp(-r/H) of the ionospheric pressure.

This qualitative consideration is illustrated by Figure 8, where the zenith angle of the line separating regions of the magnetosphere in which different pressure terms dominate is plotted as a function ρV^2 for the above discussed two variants of the model. As follows from the curves presented in Figure 8, magnetic pressure can dominate ionospheric pressure at large zenith angles even in the case of the very large solar wind ram pressure.

As mentioned previously, the smooth curve in Figures 4b and 6b can be approximately interpreted as the height profile of the sum of magnetic and ionospheric pressures in the subsolar mag-

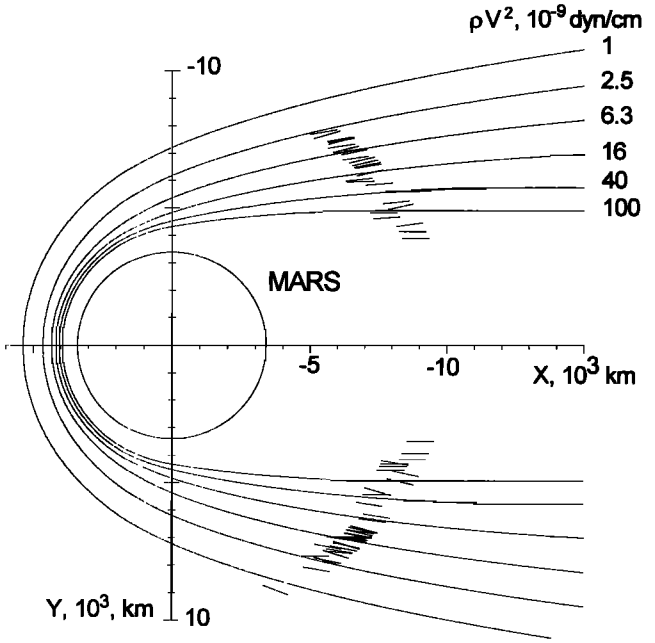

Figure 7. Variation of the modeled shape of the Martian magnetopause with the increase of solar wind ram pressure. The short lines are centered on the individual magnetopause crossings and they are inclined to the X axis at their deduced flaring angles.

netosphere multiplied by the factor of $1/k$. The low-altitude part of this curve represents the ionospheric pressure profile multiplied by the same factor.

Can the electrons and ions of the Martian ionosphere really provide a pressure larger than $(1\text{-}3)\times10^{-8}$ dyn cm^{-2} at heights of 700-800 km in the period of maximum solar activity? In fact, reliable information on the pressure distribution in the Martian ionosphere for the maximum solar activity period is not available. Owing to a lack of temperature observations or models for this case, *Zhang and Luhmann* [1992] could estimate only the lower limit of the peak ionospheric pressure as $(0.5\text{-}1.5)\times10^{-8}$ dyn cm^{-2} at zenith angles of about 75°. They considered this estimation for the period of maximum solar activity as the most speculative part of their work. The lower limit of the peak ionospheric pressure will be as high as $(1\text{-}3)\times10^{-8}$ dyn cm^{-2} when extrapolated by Chapman's theory to the subsolar point.

Even if the peak ionospheric pressure was assumed to be much higher than that quoted above for the period of the Phobos 2 observations (this assumption is not unfounded since the bow shock and magnetopause in the tail region were observed also in cases when the external ram pressure was as high as 10^{-7} dyn cm^{-2}), the ability to produce a sufficiently large pressure at the magnetopause is disputable. The problem could be resolved by the existence of a warm plasma layer with a thickness of a few hundred kilometers, with a temperature $\leq$ 10 eV, and with a density $\leq$ 1000 cm^{-3}.

The existence of such a layer and its plasma properties have not been reliably identified. The sensitivity of radio occultation measurements of electron density height profiles ($\approx 10^3$ cm^{-3}) was not sufficient to do it (see the review of Martian radio occultations by *Zhang et al.* [1990]). The Phobos 2 electric field probe measurements [*Pedersen et al.*, 1991] found a drop in the spacecraft potential to very low values after the dayside magnetopause crossing when entering the magnetosphere thus indicating a dense plasma region there. The density of this plasma was estimated sometimes as high as $\approx$ 700 cm^{-3}, but there is no information on temperature [*Grard et al.*, 1989; *Pedersen et al.*, 1991]. In the magnetic barrier region located outside the magnetopause, electric field probes observed a depletion in the plasma density (indicated by the local peak of spacecraft potential) [*Pedersen et al.*, 1991] accompanied by an increase in the magnetic field resembling the magnetic barrier region at Venus [*Zhang et al.*, 1991].

The model presented above for the Martian magnetopause is based on the pressure balance equation in order to minimize the number of free parameters to be determined. The disadvantage of such an approach is the necessity of some a priori assumptions. The purely empirical approach, used by *Sibeck et al.* [1991] and *Roelof and Sibeck* [1993] for the Earth's magnetopause shape determination is free from a priori assumptions but requires much more observational material which is not available for the case of the Martian magnetopause.

The magnetopause crossings described by this model were obtained during solar maximum, dictating our use of the ionospheric scale height relevant to the period. Since the scale height of the upper Martian atmosphere varies strongly with solar activity [*Bauer and Hantsch*, 1989], use of the model for other solar cycle phases will require modification to the model.

We do not claim that our model proves the existence of the Martian intrinsic dipole moment with a value of $(0.8\text{-}1.0)\times10^{22}$ G cm^3. It is hardly possible to make this statement without direct measurements of the magnetic field near the surface of the planet. The model just provides a new estimation of the Martian magnetic moment (if it is a dipole-like field) which conforms to the available magnetopause crossings as influenced by ρV^2 both in the subsolar and in the tail region, as well as to the magnetotail flaring angle dependence on the ρV^2.

Numerous estimates of the Martian magnetic moment were published since the Mariner 4 planetary flyby in 1965 [see, e.g., *Smith et al*, 1965, *Gringauz et al.*, 1977, *Slavin and Holzer*, 1982, *Luhmann et al.*, 1987]. The time history of M estimates with a number of relevant references can be found in the review paper of *Vaisberg* [1992]. The values of the Martian magnetic moment obtained in the present model are in good agreement with those published recently.

On the other hand, the discussion on the existence of an intrinsic magnetic field of Mars is not closed yet. For example, *Brecht* [1995], on the basis of his 3-D hybrid particle simula-

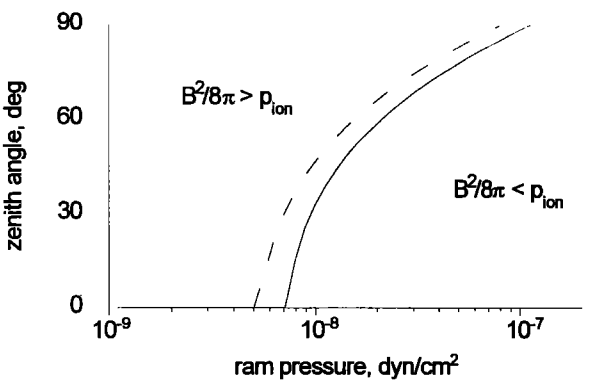

Figure 8. Position of the line separating the prevalence of the magnetospheric magnetic pressure over ionospheric pressure at the magnetopause as a function of ρV^2 in the models presented in Figure 4 (dashed line) and in Figure 6 (solid line).

tions, claimed that the dependence of the magnetotail width on ram pressure can be explained without any intrinsic magnetic field. However, some assumptions made in his simulations lead to results which in many respects do not correspond to the observations (e.g., asymmetry in magnetotail width, magnetosheath too thin).

From a formal point of view it would be possible to describe the bending in the curves of Figures 4b and 6b by taking the sum of two exponential pressure terms in the right-hand side of (4) and (5) (one of them with a scale height of the order of 10^3 km), thus having four free parameters in the optimization problem. Such an approach also could provide a reasonable description of the observations, but it would lead to unacceptably high pressures in the upper ionosphere.

Independently of the nature of the Martian obstacle to the solar wind, the model developed here for the Martian magnetopause shape can be used as a base for case studies of the Martian bow shock variations and for further studies of the magnetic field distribution in the planetary magnetosphere.

Conclusions

A model of the Martian magnetopause has been developed for the period of maximum solar activity based on TAUS ion spectrometer and MAGMA magnetometer data collected aboard Phobos 2 in February-March, 1989.

This model simultaneously describes (1) the observed relation between the solar wind ram pressure ρV^2 and the magnetopause position in the magnetotail, (2) the observed relation between ρV^2 and the flaring angle, and (3) a few magnetopause crossing observations above the dayside of the planet.

The shape of the magnetopause in the model is determined from the equation of pressure balance across this boundary when both the magnetic pressure and the ionospheric pressure are taken into account in the planetary magnetosphere. The model provides the solar zenith angle range for which the magnetic pressure exceeds the ionospheric pressure at the magnetopause for a given ram pressure.

The value of the Martian magnetic moment M was considered as one of the model's free parameters which was determined through least squares fitting from the observed magnetopause positions and corresponding solar wind ram pressure data. The optimum value of $M = (0.8\text{-}1.0)\times10^{22}$ G cm^3 seems to be practically independent of the assumed ionospheric scale height.

A specific feature of the model is the "stagnation" of the subsolar magnetopause when the ram pressure increases to values $\geq 6\times10^{-9}$ dyn cm^{-2} while the magnetotail still remains compressible up to very large ram pressures.

The model developed here for the Martian magnetopause shape can be used to study variations of the Martian bow shock and for the analysis of the magnetic field distribution in the planetary magnetosphere independently of the nature of the Martian obstacle to the solar wind.

Acknowledgments. The research described in this publication was made possible in part by grants MQU000/300 from ISF, 94-982 from INTAS, and 95-02-04223 from RFFE; by grant OTKA T 015866 of the Hungarian Science Fund; and by the Hungarian-Russian Intergovernmental S&T Cooperation Programme (Project 28).

The editor thanks P. Matheson and another referee for their assistance in evaluating this paper.

References

Aydogar, Ö., K. Schwingenschuh, G. Schelch, H. Arnold, G. Berghofer, and W. Riedler, The Phobos fluxgate magnetometer (MAGMA) instrument description, *Rep. IWF-8904*, 28 pp., Space Research Institute Austrian Acad. of Sci., Graz, Austria, 1989.

Bauer, S.J., *Physics of the Planetary Ionosphere*, 230 pp., Springer-Verlag, New York, 1973.

Bauer, S. J., and M.H. Hantsch, Solar cycle variation of the upper atmosphere temperature of Mars, *Geophys. Res. Lett.*, 16, 373-376, 1989.

Brecht, S.H., Consideration of the Martian magnetotail as evidence for an intrinsic magnetic field, *Geophys. Res. Lett.*, 22(10), 1181-1184, 1995.

Feldman, W.C., J.R. Asbridge, S.J. Bame, and J.T. Gosling, Plasma and magnetic fields from the Sun, in The Solar Wind Output and Its Variations, edited by O.R. White, pp. 351-382, Colo. Assoc. Univ. Press, Boulder, 1977,.

Grard, R., A. Pedersen, S. Klimov, S Savin, A. Skalsky, J.G. Trotignon, and C. Kennel, First measurements of plasma waves near Mars, *Nature*, 341(6243), 607-609, 1989.

Gringauz, K.I., V.V. Bezrukikh, M.I. Verigin, and A.P. Remizov, On electron and ion component of plasma in the antisolar part of near-Martian space, *J Geophys. Res.*, 81(19), 3349-3352, 1976a.

Gringauz, K.I., V.V. Bezrukikh, M.I. Verigin, L.I. Denshikova, V.I. Karpov, V.F. Kopylov, Y.D. Krysilov, and A.P. Remizov, Measurements of electron and ion plasma components along the Mars-5 satellite orbit, *Space Res*, 16, 1039-1044, 1976b.

Gringauz, K.I., V.V. Bezrukikh, T.K. Breus, M.I. Verigin, and A.P. Remizov, The magnetic field of Mars estimated from the data of plasma measurements by soviet artificial satellites of Mars, in *The Soviet-American Conference on Cosmochemistry of the Moon and Planets*, part 2, *NASA Spec. Publ. SP-370*, edited by J.H. Pomeroy and N J. Hubbard, pp. 859-863. Washington, D.C., 1977.

King, J.H., Interplanetary medium data book-Supplement 4, 1985-1988, *NSSDC/WDC-A-R&S 89-17*, NASA, Goddard Space Flight Cent., Greenbelt, Md., 1989.

Kotova, G.A., The experimental studies of the solar wind large scale structure and its interaction with Mars (in Russian), Ph.D. thesis, Space Res. Inst., Moscow, 1993.

Luhmann, J.G., C.T. Russell, F.L. Scarf, L.H. Brace, and W.C. Knudsen, Characteristics of the Mars-like limit of the Venus-solar wind interaction, *J. Geophys. Res.*, 92, 8545-8554, 1987.

Moroz V.I., V.V. Kerzhanovich, and V.V. Krasnopolsky, An engineering model of the atmosphere of Mars for the Mars-94 project (MA-90), *Cosmic. Res.*, Engl. Transl., 29, 1-79, 1991.

Paularena, K.I. and A.J. Lazarus, Comment on "Intercalibration of solar wind instruments during the International Magnetospheric Study" by S.M. Petrinec and C.T. Russell, *J. Geophys. Res.*, 99, 14,777-14,778, 1994.

Pedersen, A., C. Nairn, R. Grard, and K. Schwingenschuh, Derivation of electron densities from differential potential measurements upstream and downstream of the bow shock and in the magnetosphere of Mars, *J. Geophys. Res.*, 96(A7), 11,243-11,252, 1991.

Petrinec, S.M., and C.T. Russell, An empirical model of the size and shape of the near-Earth magnetotail, *Geophys. Res. Lett.*, 20(23), 2695-2699, 1993a.

Petrinec, S.M., and C.T. Russell, Intercalibration of solar wind instruments during the International Magnetospheric Study, *J. Geophys. Res.*, 98, 18,963-18,970, 1993b.

Petrinec, S.M. and C.T Russell, Reply to comment on "Intercalibration of solar wind instruments during the International Magnetospheric study by S.M. Petrinec and C.T.Russell, *J. Geophys Res.*, 99, 14,779-14,780, 1994.

Riedler, W , et al., Magnetic field near Mars: First results, *Nature*, 341(6243) 604-607, 1989.

Roelof, E.C., and D.G. Sibeck, Magnetopause shape as a bivariate function of the interplanetary magnetic field B_Z and solar wind dynamic pressure, *J. Geophys. Res.*, 98, 21,421-21,431, 1993.

Rosenbauer, H., et al., The study of three dimensional distribution functions of the main solar wind ions - protons and alpha-particles - in the Phobos mission. TAUS experiment (MPK instrumentation) (in Russian), in The Instrumentation and Methods in Space Research, edited by V.M. Balebanov, pp. 30-43, Nauka, Moscow, 1989a.

Rosenbauer, H., et al., Ions of Martian origin and plasma sheet in the Martian magnetotail: Initial results of TAUS experiment, *Nature*, 341(6243), 612-614, 1989b.

Rosenbauer, H., et al., The relationship between the magnetic field in the Martian magnetotail and upstream solar wind parameters, J. Geophys Res., 99(A9), 17,199-17,204, 1994.

Russell, C.T., and S.M. Petrinec, On the relative intercalibration of solar wind instruments on IMP-8 and ISEE-3, *Geophys. Res. Lett.*, 19, 961-963, 1992.

Schield, M.A., Pressure balance between solar wind and magnetosphere, *J. Geophys. Res.*, 74, 1275-1286, 1969.

Schwingenschuh, K., et al., The Martian magnetic field environment: Induced or dominated by an intrinsic magnetic field?, *Adv. Space Res.*, 12(9), 213-219, 1992.

Sibeck, D.G., R.E. Lopez, and E.C. Roelof, Solar wind control of the magnetopause shape, location and motion, *J. Geophys. Res.*, 96, 5489-5499, 1991.

Slavin, J.A., and R.E. Holzer, The solar wind interaction with Mars revisited, *J. Geophys. Res.*, 87(B12), 10,285-10,296, 1982.

Slavin, J.A., R.E. Holzer, J.R. Spreiter, S.S. Stahara, and D.S. Shaussee, Solar wind flow about the terrestrial planets, 2, Comparison with gasdynamic theory and implications for solar-planetary interactions, *J. Geophys. Res*, 88(A1), 19-35, 1983.

Slavin, J., M. Verigin, K. Gringauz, G. Kotova, S. Stahara, J. Spreiter, W. Riedler, K. Schwingenschuh, H. Rosenbauer, and S. Livi, The solar wind interaction with Mars: Phobos-2 bow shock observations on 24 March 1989, in *Plasma Environments of Non-Magnetic Planets, COSPAR Colloq. Ser.*, vol.4, edited by T.I. Gombosi, pp. 279-283, Pergamon Press, Tarrytown, N. Y., 1993.

Smith, E.J., L. Davis, Jr., P.J. Coleman Jr., and D.E. Jones, Magnetic field measurements near Mars, *Science*, 149, 1241-1242, 1965.

Spreiter, J R., A.L. Summers, and A.Y. Alksne, Hydromagnetic flow around the magnetosphere, *Planet. Space Sci.*, 14, 223-253, 1966.

Spreiter, J.R., A.L. Summers, and A.W. Rizzi, Solar wind flow past nonmagnetic planets - Venus and Mars, *Planet. Space Sci.*, 18, 1281-1299, 1970.

Tsyganenko, N.A., Modelling the Earth's magnetospheric magnetic field confined within a realistic magnetopause, *J. Geophys. Res.*, 100(A4), 5599-5612, 1995.

Vaisberg, O.L., The solar wind interaction with Mars: A review of results from previous soviet missions to Mars, *Adv. Space Res.*, 12(9), 137-161, 1992.

Verigin, M.I., et al., The dependence of the Martian magnetopause and bow shock on solar wind ram pressure according to Phobos 2 TAUS ion spectrometer measurements, *J. Gephys Res.*, 98(A2), 1303-1309, 1993

Zhang, M.H.G., and J.G. Luhmann, Comparison of the peak ionosphere pressure at Mars and Venus with incident solar wind dynamic pressure, *J. Geophys. Res.*, 97(E1), 1017-1025, 1992.

Zhang, M.H.G., J.G. Luhmann, A.J. Kliore, and J. Kim, A post Pioneer Venus reassessment of the Martian dayside ionosphere as observed by radio occultation methods, *J. Geophys. Res.*, 95(B9), 14,829-14,839, 1990.

Zhang, T.-L., J.G. Luhmann, and C.T. Russell, The magnetic barrier at Venus, *J. Geophys. Res*, 96(A7), 11,145-11,153, 1991.

Zhang, T.-L., K. Schwingenschuh, C.T. Russell, J.G. Luhmann, H. Rosenbauer, M.I. Verigin, and G.A. Kotova, The flaring of the Martian magnetotail observed by the Phobos 2 spacecraft, *Geophys. Res. Lett.*, 21(12), 1121-1124, 1994.

Zhang, T.-L., K. Schwingenschuh, S.M. Petrinec, C.T. Russell, J.G. Luhmann, H. Rosenbauer, M.I. Verigin, and G.A. Kotova, Studies of the draping and flaring angles of the Mars and Earth magnetotails, *Adv Space Res.*, 16(4), 99-103, 1995.

I. Apathy, KFKI Atomic Energy Research Institute, P.O. Box 49, 1525 Budapest, Hungary.(e-mail: apathy@sunserv.kfki.hu)

G. Kotova, A. Remizov, N. Shutte, and M. Verigin, Space Research Institute, Profsoyuznaya 84/32, Moscow 117810, Russia. (e-mail: gkotova@vmcom.lz.space.ru; aremizov@vmcom.lz.space.ru; nshutte@vmcom.lz.space.ru; mverigin@esoc1.iki.rssi.ru)

J Lemaire, Belgisch Instituut voor Ruimte-Aeronomie, Ringlaan 3, B-1180, Brussels, Belgium. (e-mail: jl@plasma.oma.be)

S. Livi, A.K. Richter, and H. Rosenbauer, Max-Planck-Institut für Aeronomie, D-37191 Katlenburg-Lindau, Germany. (e-mail: slivi@linax1.mpae.gwdg.de; rosenbauer@linax1.mpae.gwdg.de)

K. Schwingenschuh and T.-L. Zhang, Space Research Institute, Inffeldgasse 12, 8010 Graz, Austria. (e-mail: schwingen@fiwf01.tu-graz.ac.at; zhang@fiwf02.tu-graz.ac.at)

J. Slavin, NASA Goddard Space Flight Center, Code 696, Greenbelt MD 20771. (e-mail: slavin@lepjas.gsfc.nasa.gov)

K. Szegö and M. Tatrallyay, KFKI Research Institute for Particle and Nuclear Physics, 1525 Budapest P.O. Box 49, Hungary. (e-mail: szego@rmki.kfki.hu; mariella@rmki.kfki.hu)

(Received June 19, 1995; revised May 6, 1996;
accepted May 6, 1996.)